Selective Compensation Strategies for the 3-phase Cascaded Multilevel Active Power Filter using ANF-based Sequence Decoupling Scheme

Lin Xu[1], Yang Han[1, 2], Jun-min Pan[1], Chen Chen[1], Gang Yao[1], Li-Dan Zhou[1]

[1]Room 601, No.7 Dormitory, Xu Hui Campus, Shanghai JiaoTong University, Hua Shan Road #1954,
Shanghai, P. R. China, phone: +086-21 62933514; e-mail: hanyang_facts@hotmail.com
[2]School of Mechatronics Engineering, University of Electronic Science and Technology of China,
North JianShe Road, #2-4, Chengdu, P. R. China

Introduction

The power quality issues have received considerable attention in recent decades due to the increasing power quality problems in the electric distribution systems, such as: low power factor (PF), poor voltage profile, voltage fluctuations, voltage sag/swell, load unbalancing, and supply interruptions. As a result, many power quality standards were proposed, such as the IEEE 519-1992, IEEE Std.141-1993, IEEE Std.1159-1995 and IEC 1000-3-2, etc. [1-3]. Among all forms of the power quality issues, the harmonics, voltage fluctuations and sag/swell problems were recognized as the most costly events in the modern assembly lines [2, 3]. To tackle these problems, the static synchronous compensator for the distribution system (DSTATCOM) and the active power filters (APFs) [4-6] were introduced, which share the same power-stage topologies, only different in control strategy and reference current generation (RCG) schemes [4, 5]. Generally, the DSTATCOMs compensate only the fundamental reactive power while APFs compensate both fundamental reactive power and the harmonic components. Hence the APFs have received considerable attention due to the urgent requirement for tackling power quality problems [3-6].

To meet the requirement for the high-power, medium-voltage electric distributions systems, the conventional three-phase three-wire or four-wire APF topologies have evolved into the multilevel and multi-cell topologies [6]. The cascaded H-bridge (CHB) configuration is recognized as the most promising candidate among the multilevel topologies, which show the characteristic of modular capability, simple layout, excellent redundant operation ability and it can be extended to higher voltage levels by adding new modules [6]. However, the dc-link voltages across each H-bridge would tend to diverge due to unequal power losses for the individual H-bridges and the phase shift of the PWM carriers, which imposes remarkable challenges for controller synthesis. Moreover, in order to meet the requirement of the harmonic and reactive compensation for the 3-phase 3-wire systems of the

medium voltage distribution systems, the cascaded APF must be connected in delta-connection to cope with load unbalance (Fig.1). Therefore, reference signal generation for each phase leg is rather complex due to the 30 degree phase shift between the detected load currents and the synthesized reference currents.

To tackle the aforementioned problems, the individual harmonic component of load currents are decomposed by using the adaptive notch filter (ANF) in the synchronous reference frame (SRF), and the positive-sequence and negative-sequence components of individual harmonic components are successfully decoupled. After stringent mathematical manipulation of the weights of the ANF blocks in d-axis and q-axis of the SRF, the sequence components of the individual harmonic components are reconstructed by using the ANF-based technique. Hence the delta-connected multilevel APF is controlled as the single-phase multilevel APF, which significantly reduces the controller design and synthesis. Furthermore, the well-known proportional-resonant (PR) controller is utilized as current regulator to achieve zero steady state error at the selected harmonic components. And the average voltage controllers (AVCs) are used to regulate the active power flow of the cascaded H-bridges among each phase leg, and the voltage balance controllers (VBCs) are used to adjust the reactive power distribution among the individual H-bridge modules across each phase leg.

Control strategies for the three-phase multilevel APF

Fig.2 shows the controller architecture for the proposed 3-phase multilevel APF, which consists of the phase-locked loop (PLL) [7], reference current generation (RCG), current tracking and voltage balancing control units. The phase-locked loop (PLL) is based on the linear optimal adaptive filter, which achieves grid synchronization for the multilevel inverter with the grid [7, 9]. The reference current generation (RCG) schemes were reported in many previous literatures [4-6]. However, those techniques cannot be directly applied for the present system since the

individual harmonic component generated by the RCG schemes should be phase shifted by +30 or -30 degrees for the delta-connected multilevel APF, corresponding to the positive sequence or negative sequence of the considered harmonic component. This issue is solved by the ANF-based sequence decoupling scheme, which is applied in the synchronous reference frame for the load currents.
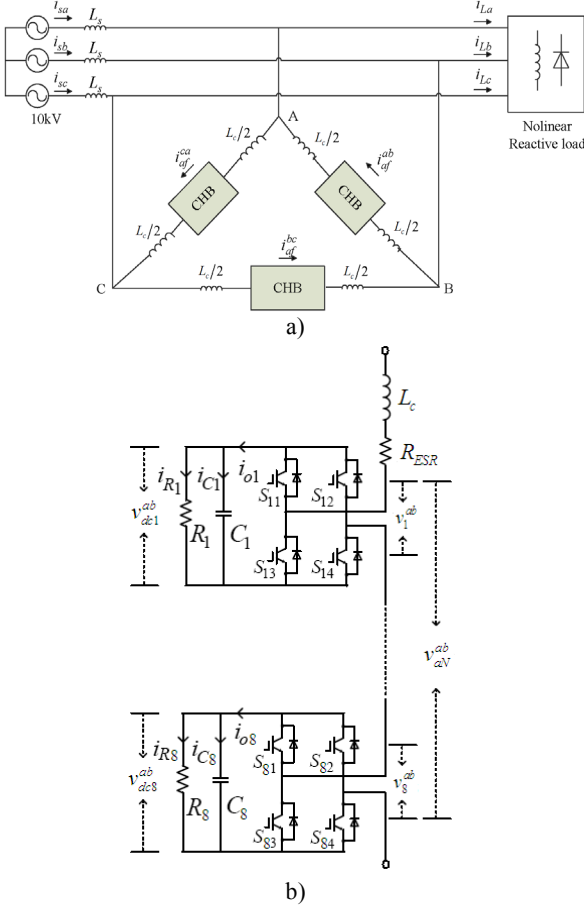

a)

b)

Fig. 1. The schematic of the three-phase multilevel APF based on cascaded H-bridge inverter (a) Overview of the proposed system; (b) Detailed illustration of the brunch between phases 'a' and 'b'
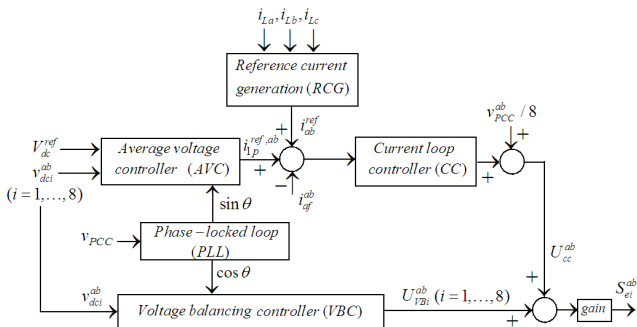

Fig. 2. Control strategies for the three-phase multilevel APF

The ANF-based sequence-decoupling technique

Fig.3 show the flowchart of the ANF-based sequence decoupling technique, and the detail illustration of the ANF is depicted in Fig.4. It is assumed that the load currents are composed of generic harmonic components, which are represented as [7]:

$$
\begin{cases}
i_{La}(t) = I_L^{+1} \cos(\omega t + \varphi^{+1}) + \sum_{m=-1,\dots\pm N} I_L^m \cos(m\omega t + \varphi^m), \\
i_{Lb}(t) = I_L^{+1} \cos(\omega t - \dfrac{2\pi}{3} + \varphi^{+1}) + \sum_{m=-1,\dots\pm N} I_L^m \cos(m\omega t - \dfrac{2\pi}{3} + \varphi^m), \\
i_{Lc}(t) = I_L^{+1} \cos(\omega t + \dfrac{2\pi}{3} + \varphi^{+1}) + \sum_{m=-1,\dots\pm N} I_L^m \cos(m\omega t + \dfrac{2\pi}{3} + \varphi^m),
\end{cases}
\tag{1}
$$

where m can be either positive or negative with ω the fundamental utility frequency, φ^{+1} and φ^m are the initial phase angle of the fundamental and mth order component, respectively, which can be expressed as [7-9]:

$$
\varphi^{+1} = \theta_1 + \Delta\theta_1, \quad \varphi^m = m\varphi^{+1} + \Delta\theta_m,
\tag{2}
$$

where θ_1 and $\Delta\theta_1$ represent the estimated phase angle of the fundamental component of the grid voltage and the estimation error, respectively, obtained from PLL, and the phase angle of the mth order harmonic component φ^m is derived in terms of the phase angle of the fundamental grid voltage and the error signal $\Delta\theta_m$.
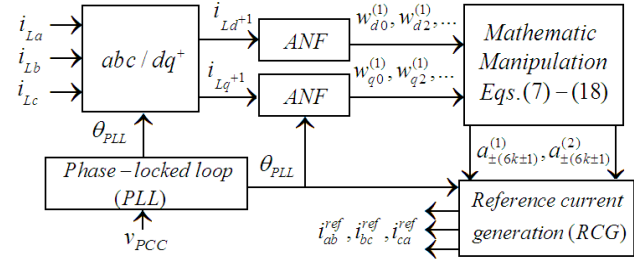

Fig. 3. The flowchart of the ANF-based sequence decoupling technique
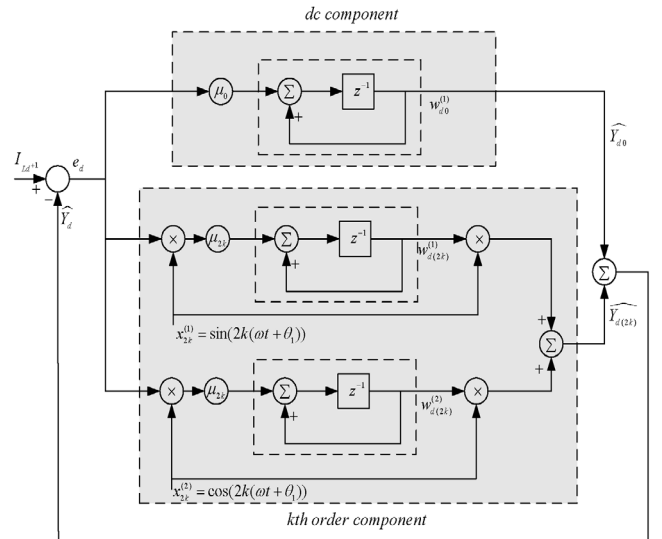

Fig. 4. The detailed diagram of the adaptive notch filter (ANF)

Hence the three-phase load currents can be transformed into synchronous frame by using Park's transformation, the d-axis and q-axis current i_{Ld}^{+1}, i_{Lq}^{+1} can be derived as:

$$
i_{Ld}^{+1} = I_L^{+1} \cos(\omega t + \varphi^{+1} - \theta_{PLL}) + \sum_{m=-1,\dots\pm N} I_L^m \cos(m\omega t + \varphi^m - \theta_{PLL}),
\tag{3}
$$

$$
i_{Lq}^{+1} = I_L^{+1} \sin(\omega t + \varphi^{+1} - \theta_{PLL}) + \sum_{m=-1,\dots\pm N} I_L^m \sin(m\omega t + \varphi^m - \theta_{PLL}),
\tag{4}
$$

If an accurate synchronization of the PLL is achieved, i.e., $\theta_{PLL} = \omega t + \theta_1$., Eq. (2) can be substituted into Eqs.(3)-(4), rearranging terms, we get：

$$i_{Ld^{+1}} = I_L^{+1}\cos(\Delta\theta_1) + \sum_{m=-1,\dots\pm N} I_L^m\cos(m\omega t + \varphi^m - \omega t - \theta_1) =$$
$$= I_L^{+1}\cos(\Delta\theta_1) + \sum_{m=-1,\dots\pm N} I_L^m\cos[(m-1)(\omega t + \theta_1) + \varphi^m - m\theta_1] = \quad (5)$$
$$= I_L^{+1}\cos(\Delta\theta_1) + \sum_{m=-1,\dots\pm N} I_L^m\cos[m\Delta\theta_1 + (\varphi^m - m\varphi^{+1})]\cos[(m-1)(\omega t + \theta_1)] -$$
$$- \sum_{m=-1,\dots\pm N} I_L^m\sin[m\Delta\theta_1 + (\phi^m - m\varphi^{+1})]\sin[(m-1)(\omega t + \theta_1)] \,,$$

$$i_{Lq^{+1}} = I_L^{+1}\sin(\Delta\theta_1) + \sum_{m=-1,\dots\pm N} I_L^m\sin(m\omega t + \varphi^m - \omega t - \theta_1) =$$
$$= I_L^{+1}\sin(\Delta\theta_1) + \sum_{m=-1,\dots\pm N} I_L^m\cos[m\Delta\theta_1 + (\varphi^m - m\varphi^{+1})]\sin[(m-1)(\omega t + \theta_1)] + \quad (6)$$
$$+ \sum_{m=-1,\dots\pm N} I_L^m\sin[m\Delta\theta_1 + (\phi^m - m\varphi^{+1})]\cos[(m-1)(\omega t + \theta_1)] \,.$$

The characteristic harmonics of the order $m=\pm(6k\pm1)$ (k is integer) are considered in this paper. To simplify the derivations, the following abbreviations are assumed:

$$\begin{cases} a_m^{(1)} = I_L^m\sin[m\Delta\theta_1 + (\phi^m - m\varphi^{+1})], \\ a_m^{(2)} = I_L^m\cos[m\Delta\theta_1 + (\phi^m - m\varphi^{+1})]. \end{cases} \quad (7)$$

For the sake of brevity, Eqs.(5)-(6) can be rewritten as:
$$\hat{Y}_d = W_d X \,, \quad \hat{Y}_q = W_q X \,, \quad (8)$$
where the weight vector W_d, W_q and the input vector X of the ANF can be denoted as [4, 5, 7]:
$$W_d = [w_{d0}^{(1)}, w_{d2}^{(1)}, w_{d2}^{(2)}, w_{d4}^{(1)}, w_{d4}^{(2)}, \dots] =$$
$$= [a_1^{(2)}, a_{-1}^{(1)}, a_{-1}^{(2)}, -a_5^{(1)}, a_5^{(2)}, (-a_7^{(1)} + a_{-5}^{(1)}), (a_7^{(2)} + a_{-5}^{(2)}), \quad (9)$$
$$\dots a_{-6k-1}^{(1)}, a_{-6k-1}^{(2)}, -a_{6k-1}^{(1)}, a_{6k-1}^{(2)}, (-a_{6k+1}^{(1)} + a_{-6k+1}^{(1)}), (a_{6k+1}^{(2)} + a_{-6k+1}^{(2)}), \dots],$$

$$W_q = [w_{q0}^{(1)}, w_{q2}^{(1)}, w_{q2}^{(2)}, w_{q4}^{(1)}, w_{q4}^{(2)}, \dots] =$$
$$= [a_1^{(1)}, -a_{-1}^{(2)}, a_{-1}^{(1)}, a_5^{(2)}, a_5^{(1)}, (a_7^{(2)} - a_{-5}^{(2)}), (a_7^{(1)} + a_{-5}^{(1)}), \quad (10)$$
$$\dots - a_{-6k-1}^{(2)}, a_{-6k-1}^{(1)}, a_{6k-1}^{(2)}, a_{6k-1}^{(1)}, (a_{6k+1}^{(2)} - a_{-6k+1}^{(2)}), (a_{6k+1}^{(1)} + a_{-6k+1}^{(1)}), \dots],$$

$$X = [1, \sin[2(\omega t + \theta_1)], \cos[2(\omega t + \theta_1)], \dots]^T \,. \quad (11)$$

The weight vector can be readily obtained from the ANF, however, when reconstructing the reference signals for the current loop controller, the parameters in Eq.(7) needs to be calculated, which can be obtained from Eqs.(9)-(10), as:

$$a_{-6k-1}^{(1)} = w_{d(6k-4)}^{(1)}, a_{-6k-1}^{(2)} = w_{d(6k-4)}^{(2)} \,, \quad (12)$$
$$a_{6k-1}^{(1)} = -w_{d(6k-2)}^{(1)}, a_{6k-1}^{(2)} = w_{d(6k-2)}^{(2)} \,,$$

$$\begin{cases} w_{d(6k)}^{(1)} = -a_{6k+1}^{(1)} + a_{-6k+1}^{(1)}, \\ w_{d(6k)}^{(2)} = a_{6k+1}^{(2)} + a_{-6k+1}^{(2)} \,, \\ w_{q(6k)}^{(1)} = a_{6k+1}^{(2)} - a_{-6k+1}^{(2)} \,, \\ w_{q(6k)}^{(2)} = a_{6k+1}^{(1)} + a_{-6k+1}^{(1)} \,. \end{cases} \quad (13)$$

From Eq.(13), we get:

$$\begin{cases} a_{6k+1}^{(1)} = \frac{1}{2}\left[w_{q(6k)}^{(2)} - w_{d(6k)}^{(1)} \right], \\ a_{6k+1}^{(2)} = \frac{1}{2}\left[w_{d(6k)}^{(2)} + w_{q(6k)}^{(1)} \right], \\ a_{-6k+1}^{(1)} = \frac{1}{2}\left[w_{d(6k)}^{(1)} + w_{q(6k)}^{(2)} \right], \\ a_{-6k+1}^{(2)} = \frac{1}{2}\left[w_{d(6k)}^{(2)} - w_{q(6k)}^{(1)} \right]. \end{cases} \quad (14)$$

An arbitrary load current in phase 'a' can be denoted as:
$$I_L^m\cos(m\omega t + \phi^m) =$$
$$= I_L^m\cos(m\omega t + \phi^m + m(\theta_1 + \Delta\theta - \varphi^{+1})) =$$
$$= I_L^m\cos(m\Delta\theta_1 + \phi^m - m\varphi^{+1} + m(\omega t + \theta_1)) = \quad (15)$$
$$= I_L^m\cos[m\Delta\theta_1 + (\phi^m - m\varphi^{+1})]\cos[m(\omega t + \theta_1)] -$$
$$- I_L^m\sin[m\Delta\theta_1 + (\phi^m - m\varphi^{+1})]\sin[m(\omega t + \theta_1)] \,.$$

From Eq.(7) and Eq.(15), we get:
$$I_L^m\cos(m\omega t + \phi^m) = a_m^{(2)}\cos(m(\omega t + \theta_1)) - a_m^{(1)}\sin(m(\omega t + \theta_1)) \quad (16)$$

For the mth order harmonic of the load currents, the reference current for the delta-connected multilevel APF can be denoted as:

$$i_{ab,m}^{ref} = I_L^m / \sqrt{3}\cos(m\omega t + \phi^m - \pi/6) =$$
$$= 1/\sqrt{3}\, a_m^{(2)}\cos(m(\omega t + \theta_1)) - \pi/6) - \quad (17)$$
$$- 1/\sqrt{3}\, a_m^{(1)}\sin(m(\omega t + \theta_1)) - \pi/6) \,.$$

Therefore, the reference compensating currents for each brunch (link-AB, -BC, -CA in Figs.1-2) are denoted as:

$$i_x^{ref} = \sum_m^{-1,\pm(6k\pm1)} i_{x,m}^{ref} \quad (x = ab, bc, ca) \,. \quad (18)$$

Current-loop control scheme

The following derivation is based on link-AB in Fig.1. However, the same result applies for other two brunches. Similar to the scheme in [6], the proportional resonant (PR) controller is utilized, which achieves perfect tracking for the alternating signals with the transfer function:

$$G_{PR}(s) = K_{cc}\{1 + \sum_{n=1}^N [\frac{1}{\tau_n} \cdot \frac{2s}{(s^2 + \omega_n^2)}]\} \,, \quad (19)$$

where the parameter τ_n (n is odd number) is defined as the time constant for the nth harmonic component of the PR controller, and ω_n denotes angular frequency of selected harmonic component. Hence, the PR regulator achieves zero steady-state error for the alternating signal at ω_n due to the infinite open-loop gain introduced by the PR current regulator. The selection of the gains and time constants for each harmonic component can be achieved by using open-loop bode-plot or closed-loop root locus diagram, which was discussed in [4-6]. Followed by the guidelines in [4, 6], the controller parameters are listed in Table 2.

In the proposed CHB-based multilevel APF, the dc-link voltage control is composed of two parts, namely, the average voltage controller, which regulates the average dc-link voltage to its reference value V_{ref}, and the voltage balancing controller, which regulates the individual dc-link voltage v_{dci} ($i=1,\dots,8$) with respect to the average dc-link voltage v_{av}.

Average voltage controller (AVC)

The AVC achieves the active power balancing between the multilevel inverter with the grid. Hence the average dc-link voltage control mimics the dc-link regulator of the existing grid-connected converters [4, 5]. Hence the AVC block in Fig.2 can be represented as:

$$i_{1p}^{ref,ab} = K_{Lim,AVC} \cdot [(V_{ref} - \frac{1}{4}\sum_{i=1}^4 v_{dci}) \cdot k_{p,AVC} \cdot (1 + \frac{1}{\tau_{AVC} \cdot s})] \cdot \sin\theta_{PLL} \,, \quad (20)$$

where $k_{p,AVC}$ and τ_{AVC} represent the controller gain and time constant of the PI regulator for the AVC, and V_{ref} denotes the reference dc-link voltage. The symbol θ_{PLL} denotes the detected phase angle of the fundamental grid voltage v_{PCC}, which is obtained from the PLL. Notably, the gain $K_{Lim,AVC}$ denotes the saturation coefficient, which limits the output of the PI regulator with a certain range to ensure a smooth operation of the system.

Table 1. The specifications of the multilevel APF

Coupling inductor (L)	6.5mH
Dc-link Capacitor (C_{dc})	2000μF
Switching frequency of IGBT (f_{sw})	2.5kHz
Sampling frequency (f_{sample})	20kHz
Grid voltage at PCC (v_{PCC})	10 kV(RMS)
Grid impedance (L_s)	0.1mH
Dc-link voltage reference (V_{dc})	2 kV

Table 2. The controller parameters for the multilevel APF

Proportional gain of PR current regulator ($k_{p,CC}$)	1.3
Time constant of PR current regulator (τ_{CC})	$12T_s$
Proportional gain of AVC($k_{p,AVC}$)	1.5
Time constant of average dc-voltage controller (τ_{AVC})	$1500T_s$
Proportional gain of voltage-balancing controller ($k_{p,VBC}$)	2.5
Time constant of voltage-balancing controller (τ_{VBC})	$2500T_s$

Voltage balancing controller (VBC)

In addition to the average voltage controller (AVC), the individual dc-link voltages across the dc capacitors should be regulated to equally share the reactive power loading. In the previous literature [10], the CHB-based inverter was utilized as reactive compensator, which has the drawback that the reactive power was not equally distributed among each H-bridge modules. In [11], the individual voltage balancing strategy (IVBS) was proposed, which achieves equal distribution of the reactive power but the controller synthesis is rather complex.

In this paper, a simple dc-link voltage balancing scheme is adopted to equally distribute reactive power among each module by exchanging active power among individual H-bridges. Whereas, the total active power absorption of the CHB-based inverter remains constant since the total active power loss is regulated by the average voltage controller (AVC). The voltage balancing controller (VBC) in Fig.2 is described as:

$$U_{VBi}^{ab} = K_{Lim,VBC} \cdot [(v_{dci}^{ab} - \frac{1}{8}\sum_{i=1}^{8} v_{dci}^{ab}) \cdot k_{p,VBC} \cdot (1+\frac{1}{\tau_{VBC} \cdot s})] \cdot \cos\theta_{PLL}, \quad (21)$$

where $k_{p,VBC}$ and τ_{VBC} represent the controller gain and time constant of the PI regulator and the gain $K_{Lim,VBC}$ denotes saturation coefficient for the VBC controller. The output of PI regulator is multiplied by a cosine function which is 90 degree phase-shifted with the fundamental component of the grid voltage, obtained from the PLL [7, 9]. From Eqs.(20)-(21), the modulation signal for the ith H-bridge of the link-AB (see Figs.1-2) is derived as:

$$S_{ei}^{ab} = [\frac{v_{PCC}^{ab}}{8} + U_{VBi}^{ab} + (i_{af}^{ref,ab} + i_{1p}^{ref,ab} - i_{af}^{ab}) \cdot G_{PR}(s)] \cdot \frac{1}{v_{dci}^{ab}}, \quad (22)$$

where $i_c^{ref,ab}$ represents the reference current of the APF generated by the ANF-based sequence decoupling block. The term $v_{PCC}/8$ denotes the grid voltage feed-forward, which is similar to the application in other grid-connected

converters in [4-6]. The obtained modulation signals are compared with individual PWM carriers to generate gating signals for the IGBTs. Notably, the PWM carriers for each H-bridge are 22.5 degree phase shifted to synthesize the multilevel output voltage for the eight H-bridge modules for each phase leg (link-AB, -BC, -CA) [6].

Simulation results and discussions

To verify the theoretical analysis, the proposed system is simulated by using Matlab/Simulink. The parameters of the power-stage and the controllers are listed in Tables 1 and 2, respectively.
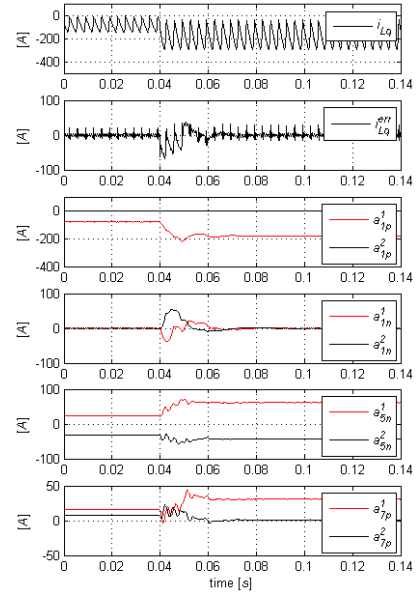

Fig. 5. Performance of the ANF-based sequence decomposition scheme under balanced load condition

Figs.5-7 show the performance of the proposed system under balanced load conditions. The three-phase diode rectifier is shunt connected with the pure inductive load to form the composite load, which undergoes a sudden step change at t=0.04s to test the dynamic performance of the system. Fig.5 shows the performance of the ANF-based sequence decoupling scheme, where the q-axis component of the load currents i_{Lq}, and the estimation error of the ANF are depicted. It can be observed that the load current i_{Lq} undergoes a sudden transient at t=0.04s, which results in a dynamic process of the estimation error of the ANF with fast decay rate. The coefficients corresponding to the positive- and negative-sequence fundamental, fifth and seventh order harmonics are depicted in Fig.5. It shows that these coefficients undergo fast transient response with less than one cycle. Besides, these coefficients are dc components in steady-state, which facilitates the current tracking performance and ensures precise compensation of the multilevel APF.

Fig.6 shows the waveforms of the grid currents, load currents and the grid voltages. It can be observed that the grid current after compensation is exactly in phase with the grid voltage (phase to ground), i.e., the unity power factor is ensured at the source side. Besides, the transient under load variations dies out in less than one cycle, which validates excellent performance of the proposed control

algorithm. Fig.7 shows the dc-link voltages of the 3-phase multilevel APF, where the dc-link voltages across the link-AB, -BC, -CA are depicted. It shows that the profiles of the eight dc-link voltages overlap with each other, which verifies the validity of the voltage balancing controllers.
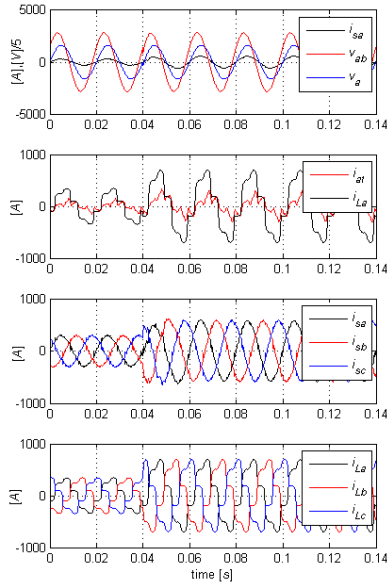

Fig. 6. The simulated grid currents, load currents and PCC voltage under balanced load condition
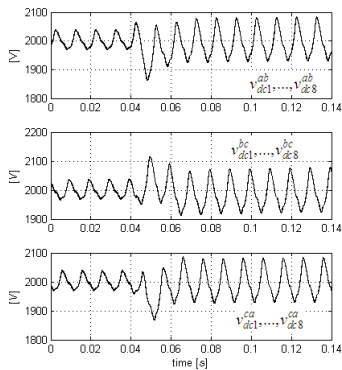

Fig. 7. The simulated dc-link voltages of the multilevel APF under balanced load condition

Figs.8-10 show the performance of the multilevel APF under unbalanced operation conditions with a transient increase of load at t=0.04s. It can be observed from Fig.8 that the q-axis of load currents shows higher fluctuations in amplitude due to a increase of the even order harmonic components resulted from load unbalance. The estimation error of the ANF is quite small in steady state with a fast dynamic response during transients. Fig.9 shows the grid currents, load currents and the grid voltage at PCC. It can be observed that the grid current is in phase with the grid voltage (phase-to-ground) at the steady state and during dynamic process, which ensures a unity power factor at the source side. It can also be noticed that the harmonic and the reactive load currents, including both the positive- and negative-sequence components, are well compensated by the proposed multilevel APF. Fig.10 shows the dc-link voltages of the multilevel APF. It shows that the eight dc-link voltages overlap with each other and the voltage fluctuations across the link-BC and –CA show higher amplitude compared to those across the link-AB. This

phenomenon is justifiable since the negative sequence components of load reactive currents are also compensated by the APF, resulting in a higher compensating current across the link-BC and link–CA.
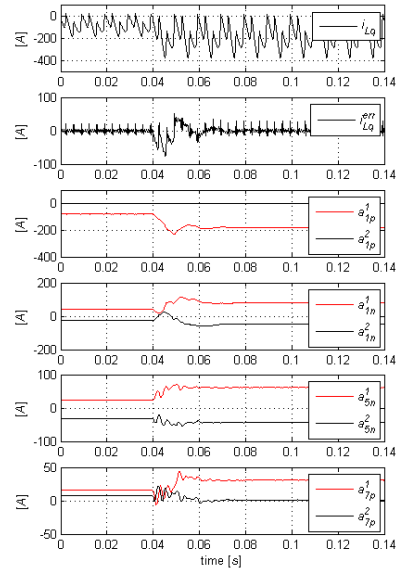

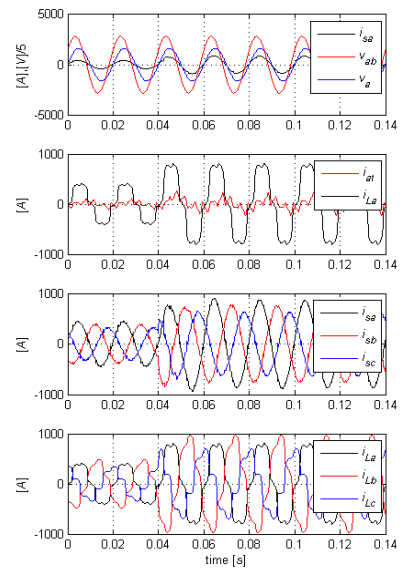**Fig. 8.** Performance of the ANF-based sequence decomposition scheme under unbalanced load condition

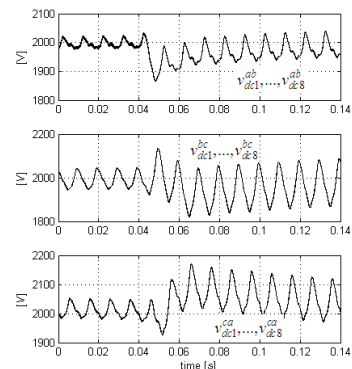**Fig. 9.** The simulated grid currents, load currents and PCC voltage under unbalanced load condition

Fig. 10. The simulated dc-link voltages of the multilevel APF under unbalanced load condition

19

Conclusions

A novel control strategy is proposed for the 3-phase multilevel cascaded APF. The selective compensation of load currents is achieved by using ANF-based sequence decoupling technique, which extract the positive-sequence and negative-sequence components of individual harmonic component in the synchronous reference frame (SRF). The theoretical analysis of the sequence decoupling scheme is outlined, followed by the design issues of the current loop regulators and the dc-link voltage controllers. The validity of the devised control scheme is verified by the simulation results under balanced and unbalanced load conditions.

References

1. **IEEE Recommended Practice for Monitoring Electric Power Quality**, IEEE Std-1159, 1995.
2. **Han Y., Xu L., Yao G., Zhou LD., Khan MM., Chen C.** Flicker mitigation of arc furnace load using modified p–q–r method // Przeglad Elektrotechniczny. – 2009. – No. 85(1). – P. 225–229.
3. **Han Y., Xu L., Yun WJ., Yao G., Zhou LD., Khan MM., Chen C.** Power quality enhancement for automobile factory electrical distribution system–strategies and field practice // Przeglad Elektrotechniczny. – 2009. – No. 85(6). – P. 159–163.
4. **Han Y., Khan M. M., Xu L., Zhou L., Yao G., Chen C.** A novel control strategy for active power filter using synchronous reference frame (SRF) ADALINEs // International Review of Electrical Engineering–IREE. – 2008. – No. 3. – P. 629–645.
5. **Han Y., Khan M. M., Zhou L., Yao G., Chen C.** A novel harmonic free power factor corrector based on T-type APF with adaptive linear neural network (ADALINE) control // Simulation Modelling Practice and Theory. – 2008. – No. 9. – P. 1215–1238.
6. **Han Y., Xu L., Yao G., Zhou LD., Khan MM., Chen C.,** Operation principles and control strategies of cascaded H-bridge multilevel active power filter // Electronics and Electrical Engineering. – 2009. – No. 3. – P. 71–76.
7. **Xu L., Han Y., Zhou LD., Yao G., Khan MM., Chen C., Pan JM.** Novel phase–locked loop using adaptive notch filter // Electronics and Electrical Engineering. – 2009. – No. 4. – P. 7–12.
8. **Han Y., Xu L., Yao G., Zhou LD., Khan MM., Chen C.,** The adaptive signal processing scheme for power quality conditioning applications based on active noise control (ANC) // Electronics and Electrical Engineering. – 2009. – No. 8. – P. 9–14.
9. **Han Y., Xu L., Khan MM., Yao G., Zhou LD., Chen C.** A novel synchronization scheme for grid–connected converters by using adaptive linear optimal filter based PLL (ALOF–PLL) // Simulation Modelling Practice and Theory. – 2009. – No. 17. – P. 1299–1345.
10. **L. YiQiao., C. O. Nwankpa.** A new type of STATCOM based on cascaded voltage-source inverters with phase-shifted unipolar SPWM // IEEE Transactions on Industry Applications. – 1999. – No. 5. – P. 1118–1123.
11. **J.A. Barrena, L. Marroyo, M. A. R. Vida, J. R. T. Apraiz.** Individual voltage balancing strategy for PWM cascaded H-bridge converter-based STATCOM // IEEE Transactions on Industry Electronics. – 2008. – No. 1. – P. 21–29.

Lin Xu, Yang Han, Jun-min Pan, Chen Chen, Gang Yao, Li–Dan Zhou. Selective Compensation Strategies for the 3-Phase Cascaded Multilevel Active Power Filter using ANF-based Sequence Decoupling Scheme // Electronics and Electrical Engineering. – Kaunas: Technologija, 2010. – No. 2(98). – P. 15–20.

A new control strategy for the 3-phase multilevel cascaded H-bridge (CHB) active power filter is presented. The selective compensation of load side reactive and harmonic components is adopted to reduce the current controller bandwidth. The adaptive notch filters (ANFs) are utilized at the d-axis and q-axis of the load side currents to extract the positive- and negative-sequence components of individual harmonic component. The theoretical derivations of the ANF-based sequence decoupling scheme is outlined, followed by the design issues of the current regulators and the dc-link voltage controllers. Simulation results under balanced and unbalanced load conditions with transient load disturbances are presented for verification. The validity of the proposed control scheme is validated by the simulation results. Ill. 10, bibl. 11 (in English; summaries in English, Russian and Lithuanian).

Лин Ху, Янг Хан, Джун-мин Пан, Чен Чен, Ганг Яо, Ли-Дан Жоу. Стратегии выборочной компенсации для трехфазного каскадного многоуровнего активного фильтра с использованием схемы развязки на основе ANF // Электроника и электротехника. – Каунас: Технология, 2010. – № 2(98). – С. 15–20.

Представлена новая стратегия управления 3-фазного каскадного многоуровнего Н-моста (CHB) активного фильтра. Принята селективная компенсация реактивной нагрузки и гармонических компонентов для сокращения текущей пропускной способности контроллера. Адаптивные фильтры ANF используются на уровне Д-оси и оси Q-токов нагрузки для извлечения положительных и отрицательных компонент последовательности отдельных гармонических компонент. Изложено теоретическое основание развязки АНФ схемы, анализированы вопросы регуляторов и DC-контроллеров напряжения. Для проверки представлены результаты моделирования в рамках сбалансированной и несбалансированной нагрузки в условиях переходных нарушений нагрузки. Действительность предлагаемой схемы контроля подтверждается результатами моделирования. Ил. 10, библ. 11 (на английском языке; рефераты на английском, русском и литовском яз.).

Lin Xu, Yang Han, Jun-min Pan, Chen Chen, Gang Yao, Li–Dan Zhou. Selektyvus trifazio kaskadinio daugiapakopio aktyvaus galios filtro kompensavimo būdai naudojant ANF pagrindu sudarytą sekos atsiejimo principą // Elektronika ir elektrotechnika. – Kaunas: Technologija, 2010. – Nr. 2(98). – P. 15–20.

Pateikiamas naujas trifazio kaskadinio H tipo tiltelio (CHB) aktyvaus galios filtro valdymo būdas. Siekiant sumažinti srovės valdiklio pralaidumo juostą, pritaikytas selektyvus apkrovos reaktyviųjų ir harmoninių komponentų kompensavimas. Teigiamiems ir neigiamiems pavienių harmonikų sekų komponentams išskirti panaudoti adaptyvieji užtvariniai filtrai (ANF). Matematiškai pagrįstas ANF grįstas sekos atsiejimo būdas, aptarti srovės ir įtampos reguliatorių projektavimo klausimai. Pateikiami modeliavimo rezultatai, esant subalansuotos ir nesubalansuotos apkrovos sąlygoms ir veikiant pereinamųjų procesų trukdžiams. Il. 10, bibl. 11 (anglų kalba; santraukos anglų, rusų ir lietuvių k.).